

# Deep Compressed Learning for 3D Seismic Inversion

Maayan Gelboim<sup>1</sup>, Amir Adler<sup>1</sup>, Yen Sun<sup>2</sup>, and Mauricio Araya-Polo<sup>2</sup>

<sup>1</sup>Braude College of Engineering, Karmiel, Israel.

<sup>2</sup>TotalEnergies EP Research & Technology US., Houston, Texas.

November 2, 2023

## 1 Summary

We consider the problem of 3D seismic inversion from pre-stack data using a very small number of seismic sources. The proposed solution is based on a combination of compressed-sensing and machine learning frameworks, known as *compressed-learning* [1, 2, 3, 4, 5, 6]. The solution jointly optimizes a dimensionality reduction operator and a 3D inversion encoder-decoder implemented by a deep convolutional neural network (DCNN). Dimensionality reduction is achieved by learning a sparse binary sensing layer that selects a small subset of the available sources, then the selected data is fed to a DCNN to complete the regression task. The end-to-end learning process provides a reduction by an *order-of-magnitude* in the number of seismic records used during training, while preserving the 3D reconstruction quality comparable to that obtained by using the entire dataset.

## 2 Introduction

Earth models can be used for many purposes, such as: seismology studies, geohazard estimation, hydrocarbon exploration and CO<sub>2</sub> sequestration. When used for CO<sub>2</sub> sequestration, subsurface models are critical inputs to analysis and decisions. Reconstruction of earth models is highly complex, involving a very large number of variables and large-scale datasets. Reconstructing 3D geological models by seismic inversion is a highly challenging task due to the huge amounts of seismic records, and the very-high computational cost of iterative numerical solution of the wave equation, as required by traditional algorithms such as Full Waveform Inversion (FWI). Just in terms of data, thousands seismic experiments are required for 3D earth model reconstruction of a typical exploration block, leading to Terabytes of recorded data.

Since the direct computation (and lack of key parameters) of the most sophisticated approximation of the wave equation is not tractable, it is common to use the inverse approach. Seismic velocity (density or others key parameters)

inversion computes a complete 3D velocity model ( $\hat{\mathbf{m}}$ ) of a certain target area, from recorded seismic data  $\mathbf{d}_r$ , and it can be summarized as:

$$\hat{\mathbf{m}} = \mathbf{G}^{-1}(\mathbf{d}_r), \quad (1)$$

where  $\mathbf{G}^{-1}$  is the inversion operator. Seismic inversion problems [7] are ill-posed, e.g., the solution is non-unique and unstable in the sense that small noise variations may alter the solution significantly. The solution of 3D seismic inversion problems using deep learning (DL) is an emerging field of research, see for example [8, 9, 10], which were motivated by state-of-the-art results obtained by DL for the 2D case [11, 12, 13, 14, 15, 16, 17, 18]. In this study we address the problem of 3D velocity inversion, while performing shots selection [19] to reduce significantly the computational load of the inversion process as well as required storage for acquired data. The proposed solution is demonstrated in an area with surface dimensions of 4.5km  $\times$  1km, which is modeled with 58 seismic experiments for 3D model reconstruction. Nevertheless, our solution is scalable to larger area dimensions and higher numbers of experiments. The target applications are: improve repeatability of seismic surveys, reduction of necessary sources for inversion algorithms (ML or other), acquisition design improvement, and inversion results explainability. Subsequent surveys of a given 4D setup can concentrate on selected sources, therefore reducing noise/mismatches coming from not selected sources. When new data is acquired the corresponding training can focus on the selected sources only, thus reducing significantly the memory and computing costs. Eventually, the collections of selected shots can be also use with other more traditional algorithms such as FWI. Knowing the most relevant sources can be incorporated in future acquisition designs, thus reducing costs. Finally, convergence and results analysis can improve by knowing exactly what sets of sources contribute the most.

### 3 Theory and Methods

Compressed Learning (CL) facilitates solutions of machine learning tasks, such as classification and regression, from compressed sensing (CS) measurements, therefore bypassing the standard requirement of full sample rate signal acquisition (either temporal or spatial). In the following we briefly explain CS and CL concepts, followed by a detailed description of the proposed solution.

**Compressed Sensing:** Given a signal  $\mathbf{x} \in \mathbf{R}^N$ , an  $M \times N$  sensing matrix  $\Phi$  (such that  $M \ll N$ ) and a measurements vector  $\mathbf{y} = \Phi\mathbf{x}$ , the goal of CS is to recover the signal from its measurements. The sensing rate is defined by  $R = M/N$ , and since  $R \ll 1$  the recovery of  $\mathbf{x}$  is not possible in the general case. According to CS theory [20], signals that have a sparse representation in the domain of some linear transform can be exactly recovered with high probability from their measurements: let  $\mathbf{x} = \Psi\mathbf{c}$ , where  $\Psi$  is the inverse transform, and  $\mathbf{c}$  is a sparse coefficients vector with only  $S \ll N$  non-zeros entries, then the recovered signal is synthesized by  $\hat{\mathbf{x}} = \Psi\hat{\mathbf{c}}$ , and  $\hat{\mathbf{c}}$  is obtained by solving the following convex optimization program:

$$\hat{\mathbf{c}} = \arg \min_{\mathbf{c}'} \|\mathbf{c}'\|_1 \text{ subject to } \mathbf{y} = \Phi\Psi\mathbf{c}', \quad (2)$$

Table 1: Proposed Joint Sensing and Inversion Architecture

Block	Layer	Unit	Comments
Input	0	Seismic Cube	58 Cubes $\times$ (192 $\times$ 64 $\times$ 496)
Sensing	1	Binarized Sensing Layer	One bit per shot (i.e. cube)
Enc1	2	Conv3D(32, (5 $\times$ 5 $\times$ 5),ReLU)	+ InstanceNormalization
	3	Conv3D(32, (5 $\times$ 5 $\times$ 5),ReLU)	+ InstanceNormalization
	4	MaxPool3D	+ Dropout(0.2)
Enc2	5-7	Enc1(64)	
Enc3	8-10	Enc1(128)	
Enc4	11-13	Enc1(256)	
Enc5	14-15	Enc1(512)	without MaxPool3D
Dec1	16	ConvTrans3D(256, (2 $\times$ 2 $\times$ 2))	+ InstanceNormalization
	17	Conv3D(256, (5 $\times$ 5 $\times$ 5))	+ InstanceNormalization
	18	Conv3D(256, (5 $\times$ 5 $\times$ 5))	+ InstanceNormalization ReLU in all Conv. layers
Dec2	19-21	Dec1(128)	
Dec3	22-24	Dec1(64)	
Dec4	25-27	Dec1(32)	
	28	Conv3D(1, (1 $\times$ 1 $\times$ 1),ReLU)	Final reconstruction layer
Output	29	Velocity Model	192 $\times$ 64 $\times$ 496 grid points

where  $\|\alpha\|_1$  is the  $l_1$ -norm, which is a convex relaxation of the  $l_0$  pseudo-norm that counts the number of non-zero entries of  $\alpha$ . The exact recovery of  $\mathbf{x}$  is guaranteed with high probability if  $\mathbf{c}$  is sufficiently sparse and if certain conditions are met by the sensing matrix and the transform. While CS was originally developed for general sensing matrices, it was later extended [21] to the special case of binary sensing matrices.

**Compressed Learning:** CL was introduced by [1], which theoretically proved that direct inference from the compressive measurements  $\mathbf{y} = \Phi\mathbf{x}$  is possible with high classification accuracy. In particular, this work provided analytical results for training a linear Support Vector Machine (SVM) classifier in the CS domain. CL implementations based on deep learning were introduced by [22, 3].

In this work we implemented a compressed learning method, which *jointly* optimizes a sparse binary sensing tensor  $\Phi$  and a non-linear 3D inversion operator  $\mathcal{R}(\Phi \odot \mathbf{d}; W)$ , parameterized by a coefficients matrix  $W$ , and  $\odot$  is the element-wise multiplication operator. The shot-gathers data tensor  $\mathbf{d}$  is element-wise multiplied with the sensing tensor  $\Phi$ , which nulls most of the shots and effectively reduces the number of shot-gathers that are utilized as input for the inversion operator. The inversion operator is an encoder-decoder that maps a set of shot-gathers (sorted seismic records) to a 3D velocity model, implemented using a deep convolutional neural network (DCNN). The proposed method provides a solution to the following joint optimization problem:

$$\{\hat{\Phi}, \hat{W}\} = \arg \min_{\phi, W} \frac{1}{N} \sum_{i=1}^N \mathcal{L}(\mathbf{m}_i, \mathcal{R}(\hat{\Phi} \odot \mathbf{d}_i; W), R, R_\phi), \quad (3)$$

where  $\{\mathbf{d}_i, \mathbf{m}_i\}_{i=1}^N$  is the training-set of  $N$  pairs of shot-gathers  $\mathbf{d}_i$  and corresponding 3D velocity-models (i.e. labels)  $\mathbf{m}_i$ . The loss function  $\mathcal{L}(\mathbf{m}_i, \hat{\mathbf{m}}_i, R, R_\phi)$  measures two misfit terms: (i) the mean absolute error (MAE) between the

ground-truth velocity model (i.e. label) and the estimated one  $\hat{\mathbf{m}}_i$ , provided by the DCNN encoder-decoder reconstruction operator  $\mathcal{R}(\bullet)$ , whose input is the compressively-sensed subset of shot gathers, denoted by  $\Phi \odot \mathbf{d}_i$ ; and (ii) the squared error between the target sensing rate  $R$  ( $0 < R < 1$ ) and the learned sensing rate  $R_\phi$ . The loss function is defined as follows:

$$\mathcal{L}(\mathbf{m}_i, \hat{\mathbf{m}}_i, R, R_\phi) = \text{MAE}(\mathbf{m}_i, \hat{\mathbf{m}}_i) + \lambda(R - R_\phi)^2, \quad (4)$$

where  $\lambda > 0$  is a weight that controls the trade-off between the two misfit terms, and

$$\text{MAE}(\mathbf{m}, \hat{\mathbf{m}}) = \frac{1}{K} \sum_{j=1}^K |m_j - \hat{m}_j|, \quad (5)$$

where  $m_j, \hat{m}_j$  are the grid point entries of the (column-stacked) ground truth 3D model  $\mathbf{m}$  and the inverted 3D model  $\hat{\mathbf{m}}$ , respectively (each model with  $K$  grid points). In this work we implemented and trained a 3D convolutional encoder-decoder, inspired by the 2D U-Net architecture [23], to learn the mapping from seismic data space to 3D models space (i.e. inversion). The complete network architecture follows the implementation introduced by [8] and detailed in Table 1, with a total of 99M parameters. Note that during training the sensing layer and the subsequent layers, represented by  $\mathcal{R}(\bullet)$ , are treated as a single deep network. However, once training is complete, the sensing layer is detached from the subsequent inference layers, and used for performing signal sensing. The input of the inversion operator  $\mathcal{R}(\bullet)$ , is therefore the second layer of the end-to-end learned network. We next discuss the construction of the sensing tensor  $\Phi$ , which follows closely the concept of *binarized neural networks*, presented in [24]. Let  $\phi_w \in R^{N_s \times 1}$  be the real-valued (non-binary) weights of the trainable sensing layer, where  $N_s$  is the number of shots. In order to convert  $\phi_w$  to a binary vector, we employ a *binarization* function, that hard-thresholds the real values using a fixed threshold, resulting in the binarized vector  $\phi_b \in \{0, 1\}^{N_s \times 1}$ . Note that each bit in  $\phi_b$  corresponds to one shot, where a value of ‘0’ corresponds to discarding the shot and ‘1’ corresponds to keeping the shot. The learned sensing rate is defined as follows:

$$R_\phi = \frac{1}{N_s} \sum_{i=1}^{N_s} \phi_b(i), \quad (6)$$

where  $\phi_b(i)$  is the  $i$ -th entry of  $\phi_b$ . The sensing tensor  $\Phi$  performs gating of the input shot-gathers, according to the binarized values in  $\phi_b$ , by element-wise multiplication with the data tensor  $\mathbf{d} \in R^{N_s \times N_{rx} \times N_{ry} \times T}$ , where  $N_{rx}, N_{ry}, T$  are the number of horizontal-axis receivers, number of vertical-axis receivers and number of time-samples, respectively. Therefore, the sensing tensor  $\Phi$  is required to have identical dimensions to  $\mathbf{d}$  and it is constructed by replicating the binarized value per-shot in  $\phi_b$  for all the receivers and time-sample entries, corresponding to that specific shot in  $\Phi$ . Since the derivative of the *binarization* function has a discontinuity with an indefinite value, it cannot be utilized for back-propagation. Therefore, the forward-pass employs the binarization function, whereas the backward-pass utilizes the *hard-sigmoid* function  $\sigma_H(x)$ , defined as follows:

$$\sigma_H(x) = \max(0, \min(1, \frac{x+1}{2})), \quad (7)$$

which is linear with slope 0.5 for  $-1 \leq x \leq 1$  and has a well-defined derivative for all values of  $x$ , where  $x = \phi_w(i)$  with  $i = 1, \dots, N_s$ .

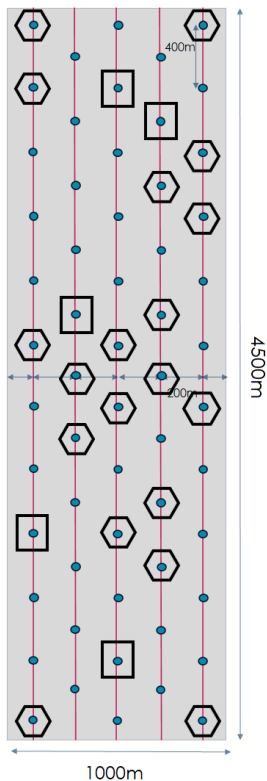


Figure 1: Geometry of the 58 shot positions (blue circles). The sensing layer selects only a fraction of the available 58 shots. The blue circles within hexagons represent the shots selected with 30% of the original shots, and the ones within squares are selected with only 10% of the original shots.

## 4 Results and Observations

Performance of the proposed approach was evaluated by generating 2000 3D models of dimensions  $4.5\text{Km} \times 1.0\text{Km} \times 4\text{Km}$  (length  $\times$  width  $\times$  depth), with variable thickness velocity layers, including random salt geometries in 40% of the models. All models were generated using the Gempy (<https://www.gempy.org/>) tool, for 3D geological modeling. Seismic surveys were simulated using an isotropic acoustic wave approximation (see [25]), 58 shots per model were arranged along 5 parallel columns, as illustrated in Figure 1, with adjacent columns separated by 200m and evenly-spaced shots per column. Acquisition geometry was set to a uniform rectangular grid of receivers, separated by 15m in the horizontal and vertical axes. All traces were further multiplied by a monotonically-increasing time-boosting function that compensates the attenuation of wave reflections from the lowest geological layers by amplifying late-arrival time samples. We split the 2000 samples (velocity models as labels and their corresponding traces as data) into 1600 training and 400 testing samples. We initially trained the DCNN without compressed sensing (CS), using our baseline system that has no sensing layer and processes the entire collection of shots. To overcome the high computational requirements of this, we utilized

the dimensionality reduction scheme, proposed in [8], in which all shot-gathers are spatially averaged along the shots dimension, resulting in a single data cube denoted by  $\bar{\mathbf{d}}(R_x, R_y, t)$ , where  $R_x, R_y$  are the indices of the receiver positions, and  $t$  is time-sample index. The dimensionality-reduced data cube is defined as follows:

$$\bar{\mathbf{d}}(R_x, R_y, t) = \frac{b(t)}{N_s} \sum_{S=1}^{N_s} \mathbf{d}(S, R_x, R_y, t), \quad (8)$$

where  $b(t)$  is a monotonically-increasing time-boosting function. Therefore,  $\bar{\mathbf{d}}$  forms a single 3D input channel, thus significantly mitigating the memory and computational requirements for training and inference of the proposed DCNN, as discussed in [8]. We further trained the joint sensing and inversion architecture, as detailed in Table 1, with target sensing rates of 30% and 10%. Note that the spatial averaging along the shots dimension was not employed to the CS shots, and each shot was processed by a separate 3D convolutional layer. Reconstructed velocity models' quality was evaluated on the testing set, using the 3D Structural Similarity Index Measure (SSIM) [26], computed by averaging the 2D SSIM's along the XY, XZ and YZ planes. 3D SSIM results evaluated on the held-out testing set were 0.9265 out of 1.0 (without CS), 0.9262 (with 30% CS rate) and 0.9225 (with 10% CS rate). Visual examples of reconstructed 2D slices are provided in figure 2(a), and of 3D models are provided in figure 2(b)-(c), clearly demonstrating the good velocity model building quality, even at a 10% compressed sensing rate. During training using 10% of the sources is drastically more computationally efficient than using all of them, but it is more expensive than using the approach in Equation 8. The advantage of using CS is that when a small set of sources is selected, the subsequent training and acquisition design will be more efficient. Further, pre-processing steps costs are reduced if one decide to use Equation 8 along with the CS selected shots, this combination yields the best solution in terms computational cost and reconstruction accuracy, plus helps to better understand the learning process in relation to the data used.

## 5 Conclusions

Seismic inversion for reconstructing 3D geological structures is a highly challenging task due to the huge amounts of acquired seismic data, and very-high computational load required for iterative numerical solutions of the wave equation, as required by Full Waveform Inversion. We presented a solution that jointly optimizes the compressed sensing operator with the 3D inversion network, leading to an order-of-magnitude reduction of the number of required shot-gathers for high-quality 3D inversion. The solution facilitates lower memory and computational requirements, and can be further extended to simplify and optimize the acquisition setup geometry.

## 6 Acknowledgments

The authors acknowledge TotalEnergies EP Research and Technology US, for supporting this work and allowing its publication.

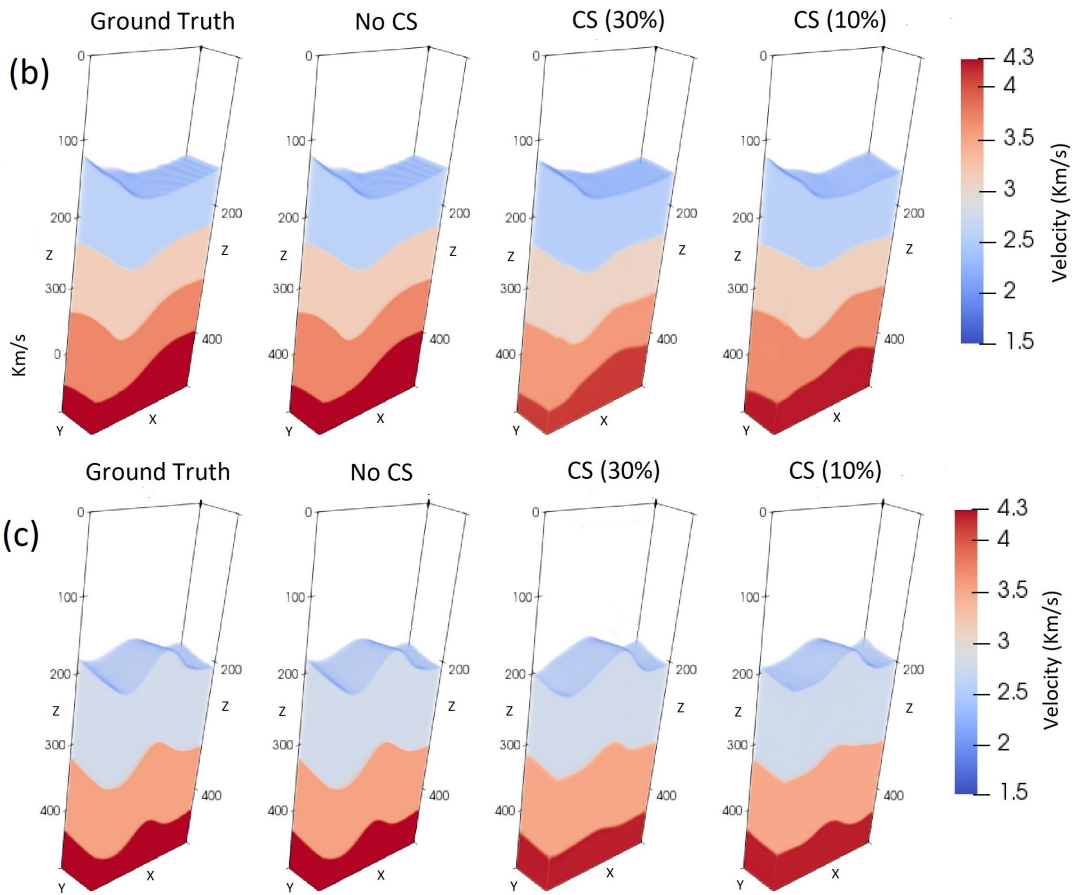
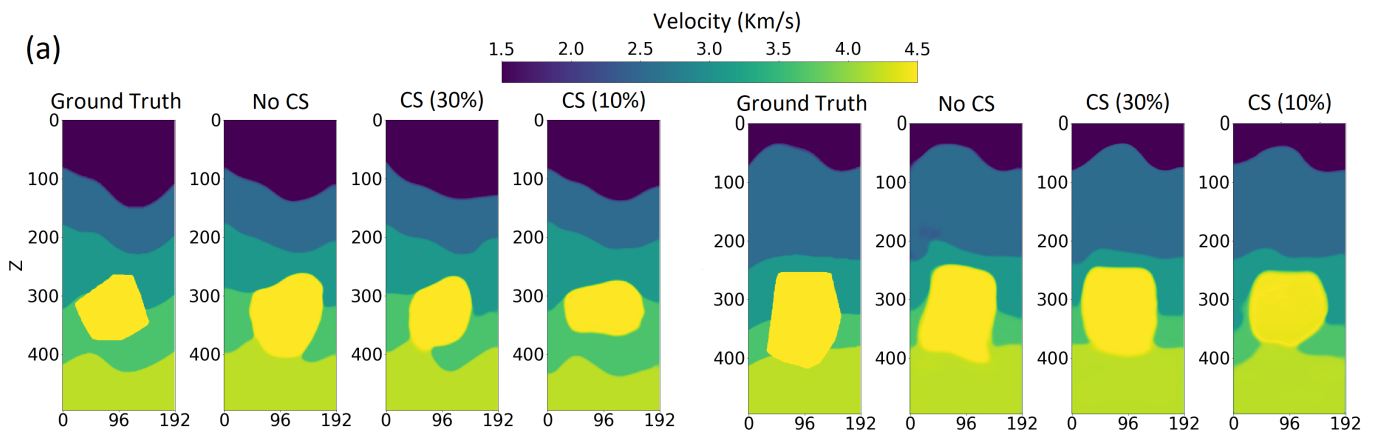


Figure 2: (a) Samples of 2D slices from 3D models testing-set, illustrating high-quality reconstructions of the variable thickness layers interfaces, and salt geometries, at sensing rates of 30% and 10%. (b) and (c) Samples of reconstructed 3D models illustrating high-quality reconstructions at sensing rates of 30% and 10%.

## References

- [1] R. Calderbank, S. Jafarpour, and R. Schapire, “Compressed learning: Universal sparse dimensionality reduction and learning in the measurement domain,” 2009.
- [2] R. Calderbank and S. Jafarpour, “Finding needles in compressed haystacks,” in *Compressed Sensing: Theory and Applications*, p. 439–484, Cambridge University Press, 2012.
- [3] E. Zisselman, A. Adler, and M. Elad, “Compressed learning for image classification: A deep neural network approach,” *Handbook of Numerical Analysis*, vol. 19, pp. 3–17, 2018.
- [4] R. Mdrafi and A. C. Gurbuz, “Compressed classification from learned measurements,” in *Proceedings of the IEEE/CVF International Conference on Computer Vision*, pp. 4038–4047, 2021.
- [5] C. Douarre, C. F. Crispim-Junior, A. Gelibert, G. Germain, L. Tougne, and D. Rousseau, “CTIS-Net: A neural network architecture for compressed learning based on computed tomography imaging spectrometers,” *IEEE Transactions on Computational Imaging*, vol. 7, pp. 572–583, 2021.
- [6] C. Mou and J. Zhang, “TransCL: Transformer makes strong and flexible compressive learning,” *IEEE Transactions on Pattern Analysis and Machine Intelligence*, vol. 45, no. 4, pp. 5236–5251, 2023.
- [7] G. T. Schuster, *Seismic Inversion*. Society of Exploration Geophysicists, 2017.
- [8] M. Gelboim, A. Adler, Y. Sun, and M. Araya-Polo, “Encoder–decoder architecture for 3D seismic inversion,” *Sensors*, vol. 23, no. 1, p. 61, 2022.
- [9] H.-f. Tan, W.-q. Li, J. Xu, and G.-a. Wei, “Deep learning 3D inversion of subsurface target based on multinary electromagnetic data,” in *Proceedings of the International Field Exploration and Development Conference 2020*, pp. 2816–2825, Springer, 2021.
- [10] Q. Zeng, S. Feng, B. Wohlberg, and Y. Lin, “Inversionnet3D: Efficient and scalable learning for 3-d full-waveform inversion,” *IEEE Transactions on Geoscience and Remote Sensing*, vol. 60, pp. 1–16, 2021.
- [11] A. Adler, M. Araya-Polo, and T. Poggio, “Deep learning for seismic inverse problems: Toward the acceleration of geophysical analysis workflows,” *IEEE Signal Processing Magazine*, vol. 38, no. 2, pp. 89–119, 2021.
- [12] F. Yang and J. Ma, “Deep-learning inversion: a next generation seismic velocity-model building method,” *GEOPHYSICS*, vol. 84, no. 4, pp. R583–R599, 2019.
- [13] M. Araya-Polo, A. Adler, S. Farris, and J. Jennings, “Fast and accurate seismic tomography via deep learning,” in *Deep learning: Algorithms and applications*, pp. 129–156, Springer, 2020.



- [14] M. J. Park and M. D. Sacchi, “Automatic velocity analysis using convolutional neural network and transfer learning,” *Geophysics*, vol. 85, no. 1, pp. V33–V43, 2020.
- [15] Z. Zhang and T. Alkhalifah, “Regularized elastic full-waveform inversion using deep learning,” in *Advances in Subsurface Data Analytics*, pp. 219–250, Elsevier, 2022.
- [16] Y. Li and T. Alkhalifah, “Target-oriented time-lapse elastic full-waveform inversion constrained by deep learning-based prior model,” *IEEE Transactions on Geoscience and Remote Sensing*, vol. 60, pp. 1–12, 2022.
- [17] G. Fabien-Ouellet and R. Sarkar, “Seismic velocity estimation: A deep recurrent neural-network approach,” *Geophysics*, vol. 85, no. 1, pp. U21–U29, 2020.
- [18] W. Zhu, K. Xu, E. Darve, B. Biondi, and G. C. Beroza, “Integrating deep neural networks with full-waveform inversion: Reparameterization, regularization, and uncertainty quantification,” *Geophysics*, vol. 87, no. 1, pp. R93–R109, 2022.
- [19] M. Araya-Polo, C. Hegde, P. Indyk, and L. Schmidt, “Greedy strategies for data-adaptive shot selection,” in *77th EAGE Conference and Exhibition 2015*, vol. 2015, pp. 1–5, EAGE Publications BV, 2015.
- [20] D. Donoho, “Compressed sensing,” *IEEE Transactions on Information Theory*, vol. 52, no. 4, pp. 1289–1306, 2006.
- [21] W. Lu, T. Dai, and S.-T. Xia, “Binary matrices for compressed sensing,” *IEEE Transactions on Signal Processing*, vol. 66, no. 1, pp. 77–85, 2018.
- [22] A. Adler, E. Zisselman, and M. Elad, “Compressed learning: A deep neural network approach,” in *Signal Processing with Adaptive Sparse Structured Representations (SPARS17)*, 2017.
- [23] O. Ronneberger, P. Fischer, and T. Brox, “U-Net: Convolutional networks for biomedical image segmentation,” in *Medical Image Computing and Computer-Assisted Intervention – MICCAI 2015*, (Cham), pp. 234–241, Springer International Publishing, 2015.
- [24] I. Hubara, M. Courbariaux, D. Soudry, R. El-Yaniv, and Y. Bengio, “Binarized neural networks,” *Advances in neural information processing systems*, vol. 29, 2016.
- [25] J. Meng, A. Atle, H. Calandra, and M. Araya-Polo, “Minimod: A finite difference solver for seismic modeling,” 2020.
- [26] Z. Wang, A. Bovik, H. Sheikh, and E. Simoncelli, “Image quality assessment: from error visibility to structural similarity,” *IEEE Transactions on Image Processing*, vol. 13, no. 4, pp. 600–612, 2004.